

Polyblur: Removing mild blur by polynomial reblurring

Mauricio Delbracio Ignacio Garcia-Dorado Sungjoon Choi Damien Kelly Peyman Milanfar
Google Research

Abstract

We present a highly efficient blind restoration method to remove mild blur in natural images. Contrary to the mainstream, we focus on removing slight blur that is often present, damaging image quality and commonly generated by small out-of-focus, lens blur, or slight camera motion. The proposed algorithm first estimates image blur and then compensates for it by combining multiple applications of the estimated blur in a principled way. To estimate blur we introduce a simple yet robust algorithm based on empirical observations about the distribution of the gradient in sharp natural images. Our experiments show that, in the context of mild blur, the proposed method outperforms traditional and modern blind deblurring methods and runs in a fraction of the time. Our method can be used to blindly correct blur before applying off-the-shelf deep super-resolution methods leading to superior results than other highly complex and computationally demanding techniques. The proposed method estimates and removes mild blur from a 12MP image on a modern mobile phone in a fraction of a second.

1. Introduction

Image sharpness is undoubtedly one of the most relevant attributes defining the visual quality of a photograph. Blur is caused by numerous factors such as the camera's focus not being correctly adjusted, objects appearing at different depths, or when relative motion between the camera and the scene occurs during exposure. Even in perfect conditions, there are unavoidable physical limitations that introduce blur. Light diffraction due to the finite lens aperture, integration of the light in the sensor and other possible lens aberrations introduce blur leading to a loss of details. Additionally, other components of the image processing pipeline itself, particularly demosaicing and denoising, can introduce blur.

Removing blur from images is a longstanding problem in image processing and computational photography spanning more than 50 years [21, 24, 27]. Progress has been clear and sustained. From image enhancement algorithms [13, 44],

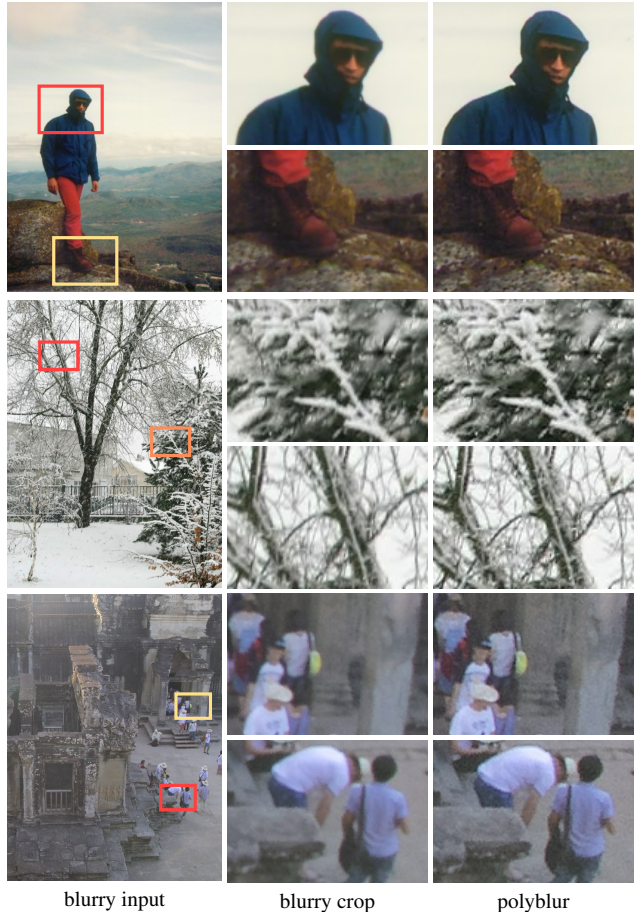


Figure 1: Mild blur, as shown in these examples, can be efficiently (42ms/MP on a mid-range smartphone CPU) removed by combining multiple applications of the estimated blur. Readers are encouraged to zoom-in for better visualization.

blind and non-blind deconvolution methods [9, 28, 38, 41] where sophisticated priors are combined with optimization schemes, to very recent years with the incipient application of deep neural models [10, 25, 26, 42, 45, 54, 48].

Many of these methods are capable of processing significantly degraded images revealing previously unseen image

details. The gain in quality is in many cases extraordinary, but impractical. These methods make extensive use of prior information (learned or modeled) producing images that are often unrealistic. This is mainly because the inverse problem they tackle is seriously ill-posed.

In this work, we detach ourselves from the current trend and focus on the particular case where the blur in the image is small. As we show in our experimental results, for this case, the vast majority of existing methods generate notorious image artifacts in addition to requiring great computational power. This is mainly because most of the algorithms were not specifically designed for this very common and practical use case. We introduce a highly efficient blind image restoration method that removes mild blur in natural images. The proposed algorithm first estimates image blur and then compensates for it by combining multiple applications of the estimated blur in a principled way. The method is inspired by the fact that the inverse of an operator that is close to the identity (e.g., mild blur), can be well approximated by means of a low-degree polynomial on the operator itself. We design polynomial filters that use the estimated blur as a base and approximate the inverse without neglecting that image noise can get amplified. The removal of blur commonly leads to the introduction of halos (oversharpening) mostly noticeable near image edges. To address this, we present a mathematical characterization of halos and propose a blending mechanism to render an artifact-free final image. This step, which is also highly efficient, is important to achieve consistent high quality.

Experiments with both real and synthetic data show that, in the context of mild blur in natural images, our proposed method outperforms traditional and modern blind deblurring methods and runs in a fraction of the time. The simplicity of the polynomial filter, together with the choice of the Gaussian function as blur the model, enables a highly efficient implementation. The method runs at interactive rates so it can be used on mobile devices. Polyblur can estimate and remove mild blur on a 12MP image on a modern mobile phone in a fraction of a second. Additionally, we show that Polyblur can be used to blindly correct blur on an image before applying an off-the-shelf deep super-resolution method. Learning-based single image super-resolution algorithms (SISR) are usually trained on images where the degradation operator has been modeled in an over-simplistic way (typically by bilinear or bicubic blur). Polyblur in combination with a standard deep SISR network leads to superior results than other highly complex and computationally demanding methods.

2. Related Work

Image blur is generally modeled as a linear operator acting on a sharp latent image. If the blur is shift-invariant then the blurring operation amounts to a convolution with a blur

kernel. This implies,

$$v = k * u + n, \tag{1}$$

where v is the captured image, u the underlying sharp image, k the unknown blur kernel and n is additive noise. In what follows we review the different families of methods that remove image blur.

Blind deconvolution and variational optimization. The typical approach to image deblurring is by formulating the problem as one of blind deconvolution where the goal is to recover the sharp image u without knowing the blur kernel k [6, 24, 27]. Most blind deconvolution methods run on two steps: a blur kernel k is first estimated and then a non-blind deconvolution technique is applied [8, 9, 35, 37, 50, 51]. Fergus et al. [9] is one of the best examples of the blind deconvolution variational family that seeks to combine image priors, assumptions on the blurring operator, and optimization frameworks, to estimate both the blurring kernel and the sharp image [4, 7, 18, 23, 31, 38, 41, 51]. Estimating the blur kernel is easier than jointly estimating the kernel and the sharp image together. Levin et al. [28, 29] show that it is better to first solve a maximum a posteriori estimation of the kernel than the latent image and the kernel simultaneously. Notwithstanding, even in non-blind deblurring, the significant attenuation of the image spectrum by the blur and model imperfections, lead to an ill-posed inverse problem [1, 22].

Sharpening methods. Sharpening methods aim to reduce mild blur and increase overall image contrast by locally modifying the image. Unsharp masking, arguably the most popular sharpening algorithm is very sensitive to noise and generally leads to oversharpening artifacts [20, 39]. Zhu and Milanfar [56] propose an adaptive sharpening method that uses the local structure and a local sharpness measure to address noise reduction and sharpening simultaneously. Bilateral filtering [47], and its many variants/adaptations [3, 13, 32, 44] can be used to enhance the local contrast and high frequency details of an image. The overall idea is to proceed similarly to that of unsharp masking: the input image is filtered and then a proportion of the residual image is added back to the original input. This procedure boosts high-frequencies that are removed by the adaptive filter. Since sharpening methods do not explicitly estimate image blur, their deblurring performance is limited. In fact, sharpening algorithms are strictly local operators and do not have access to additional information from outside the local neighborhood. Whereas deblurring algorithms like ours use the estimation of blur, which in general is global or done on a larger neighborhood, to remove the blur.

Deblurring meets deep-learning. In the past five years, with the popularization of deep convolutional networks sev-

eral image deblurring methods have been introduced [5, 10, 25, 26, 42, 43, 45, 48, 49, 54]. Most of these methods target strong motion blur and are in general trained with large datasets with realistically synthesized image blur. Efficient deblurring using deep models is a very challenging task [34].

Blind deconvolution methods do a remarkable job when the image is seriously damaged and manage to enhance very low quality images. However, their performance in the particular case where blur is mild is limited since they introduce, in general, noticeable artifacts and have a significant computational cost. At the other extreme, adaptive sharpening methods do a fine job boosting image contrast when the input image has very little blur. Since they do not incorporate any explicit measure of the blur, their deblurring capabilities are restricted. Deep learning based methods require high computational cost, making them impractical in many contexts. This work focuses on the problem of estimating and removing slight blur. As we show in the experimental part, in this setting, the proposed method produces superior results to blind deconvolution techniques and other popular adaptive sharpening algorithms, and similar results vs. advanced deep networks while being significantly more efficient.

3. Deblurring with polynomial filters

Approximating the filter inverse. Let us first assume that we have an estimation of the blur kernel k . To recover the image u we need to solve an inverse (deconvolution) problem. If the blur kernel is very large, the inversion is significantly ill-posed and some form of image prior will be required. In this work, we assume that the image blur is mild (see examples on Figure 1) so, as we will show in the experimental section, there is no need to incorporate any sophisticated image prior. Instead we proceed by building a linear restoration filter constructed from the estimated blur. An interesting observation [19, 33, 46] is that by carefully combining different iterations of the blur operator on the blurry image we can approximate the inverse of the blur.

One way to illustrate this is as follows.

Lemma 1. *Let K be the convolution operator with the blur kernel k , then if $\|I - K\| < 1$ under some matrix norm, K^{-1} the inverse of K exists and,*

$$K^{-1} = \sum_{i=0}^{\infty} (I - K)^i. \quad (2)$$

The proof is a direct consequence of the convergence of the geometric series. If we assume circular boundary conditions for the convolution, then the eigenvectors of the matrix K are the Fourier modes of k . This implies that $(I - K)^i = F^H (I - D)^i F$, where F is the Fourier basis,

F^H is the Hermitian transpose of F , and D is a diagonal matrix with the eigenvalues of K .

In particular, the series converges if the kernel Fourier coefficients $\hat{k}(\zeta)$ satisfy $|\hat{k}(\zeta) - 1| < 1$. In the case of blur filters that conserve the overall luminosity, a reasonable hypothesis is that $k(\mathbf{x}) \geq 0$, and $\int k(\mathbf{x}) d\mathbf{x} = 1$. This implies that $|\hat{k}(\zeta)| \leq 1$ which is not enough to guarantee convergence.

Polynomial filters. According to Lemma 1 we can approximate the inverse with a polynomial filter using the blur kernel as a base. For instance, if we truncate the power series and keep up to order 3, the polynomial approximate inverse of K is,

$$K_3^{\text{inv}} = 4I - 6K + 4K^2 - K^3. \quad (3)$$

This motivates the use of more general polynomials

$$p(K) = \sum_{i=0}^d a_i K^i, \quad (4)$$

where the order d and coefficients (a_0, \dots, a_d) can be designed to amplify or attenuate differently depending on how the blur is affecting a particular component.

Symmetric filters with non-negative Fourier coefficients.

Let us first assume that the blur filter $k(\mathbf{x})$ is symmetric $k(\mathbf{x}) = k(-\mathbf{x})$, and has non-negative Fourier coefficients. We will later show how we can generalize the approach to any filter. In this setting, $\hat{k}(\zeta)$ the Fourier coefficients of the filter k are in $[0, 1]$. The Fourier coefficients of the polynomial filter are related with the ones from the base filter through the same polynomial, that is,

$$\widehat{p(k)}(\zeta) = \sum_{i=0}^d a_i \hat{k}(\zeta)^i. \quad (5)$$

A polynomial filter can be analyzed in the Fourier domain by looking into how the interval $I = [0, 1]$ is mapped by the polynomial. This reflects how the differently attenuated Fourier components get amplified or attenuated by the polynomial filter. In Figure 2 we show a plot of different example polynomials $p(x)$ when applied to a signal $x \in I$.

If we apply the polynomial filter to an image v that has been affected by the same base blur k as the one used to build the polynomial filter, we get

$$p(K)v = p(K)Ku + p(K)n, \quad (6)$$

where it becomes evident that there is a trade-off between inverting the blur (i.e., $p(K)K \approx Id.$) and avoiding noise

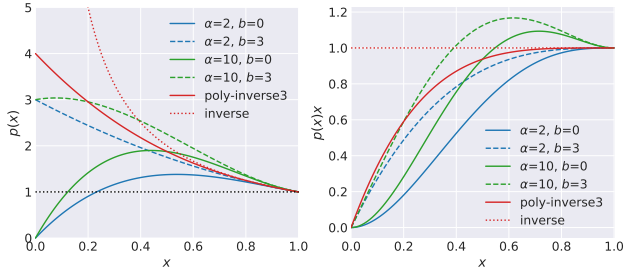


Figure 2: Polynomial filters can be analyzed directly on the *Real* line. We present an example of the proposed $p_{3,\alpha,b}$ family.

amplification, i.e., $p(K)n \approx 0$. Our goal is to design polynomials that (i) try to invert the effect of blur in the frequencies that have not been significantly attenuated, and (ii) avoid over-amplifying frequencies affected by the blur. The right plot in Figure 2 shows $p(x)x$, which can be interpreted as the combined effect of applying the polynomial on a signal that has been attenuated by the same blur.

3.1. Designing deblurring polynomial filters

We want to build a polynomial filter $p(K)K \approx Id$, when K is close to the identity, or in terms of the polynomial, $p(x) \approx 1/x$ if $x \approx 1$. Note that a Taylor expansion of $1/x$ at $x = 1$ of degree d , leads to the polynomial filter from truncating (2) to degree d . This polynomial does a good job approximating the inverse, but significantly amplifies noise, particularly in the most attenuated components. Instead, we propose to approximate the inverse but have better control of how noise is amplified. Let us assume we design a polynomial of degree d , i.e., we need to define the $d + 1$ coefficients. We will approximate the inverse by forcing the polynomial to have equal derivatives at the ones of the inverse function at $x = 1$. This is done up to order $d - 2$,

$$p^{(i)}(x = 1) = (-1)^i i!, \quad (7)$$

for $i = 1, \dots, d - 2$. We also have the additional constraint that $p(x = 1) = 1$ (no change in luminosity). The remaining two degrees of freedom are left as *design parameters*. We can control how the mid-frequencies get amplified by controlling $p^{(d-1)}(x = 1) = \alpha$, and also, how noise is amplified at the frequencies that are completely attenuated by the blur, by controlling $p(x = 0) = b$. This system of $d + 1$ linear equations leads to a (closed-form) family of polynomials, $p_{d,\alpha,b}$. The value of α and b should vary in a range close to the one given by the truncated power series, i.e., $\alpha = (-1)^d d!$ and $b = d + 1$.

We choose the polynomial filter family of degree $d = 3$,

$$p_{3,\alpha,b}(x) = (\alpha/2 - b + 2)x^3 + (3b - \alpha - 6)x^2 + (5 - 3b + \alpha/2)x + b. \quad (8)$$

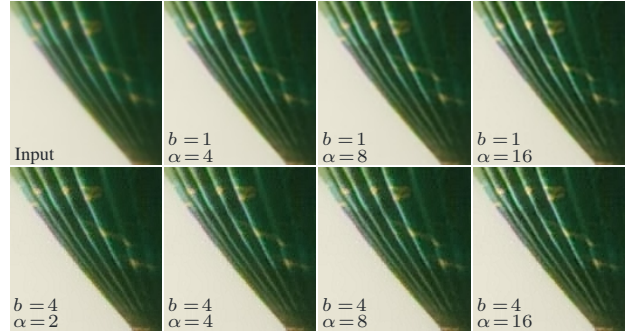


Figure 3: Effect of using different Polynomials from the $p_{3,\alpha,b}$ family.

In Figure 2 we show different polynomials and how their shape is affected by the design parameters α and b . All the results presented in this article are with polynomials of this third order family. As an illustration, we show in Figure 3 the behavior using different coefficients in the polynomial deblurring.

Generalization to any blur filter. Kernels with negative or complex Fourier coefficients (as the one shown in Fig. 4a) cannot be directly deblurred using our Polynomial filtering. Negative or complex Fourier coefficients will get wrongly amplified by the Polynomial deblurring leading to strong image artifacts (Fig. 4b). One way to circumvent this is by applying a correction filter $c_k(\mathbf{x})$ to the input image so that total blur kernel $h = c_k * k$ has the desired properties (non-negative Fourier coefficients). Thus, we proceed as follows. Given the kernel k and the blurry image v , we compute $v_c = c_k * v$, and $h = c_k * k$. Image v_c is deblurred using a polynomial filter with base filter h .

Filtering the image with the flipped kernel, i.e., $c_k(\mathbf{x}) = k(-\mathbf{x})$ will lead to $h(\mathbf{x})$ having real non-negative Fourier coefficients $\hat{h}(\zeta) = |\hat{k}(\zeta)|^2$. However, this correction filter introduces additional blur to the image, making the deblurring problem harder (Fig. 4c) An alternative approach is to design the correction filter to compensate for the *phase* but without introducing any additional attenuation of the spectra. This can be done by the pure phase filter, $\hat{c}_k(\zeta) = \tilde{k}(\zeta)/|\hat{k}(\zeta)|$. As can be shown in the example in Figure 4d, phase correction leads to a deblurred artifact-free image.

4. Parametric mild blur model and estimation

Since we target mild-blur removal, there is not much gain in having a very fine model of the blur. We thus propose to model the blur kernel with an anisotropic Gaussian function, specified with three parameters: σ_0 , the standard deviation of the main axis, $\rho = \sigma_1/\sigma_0$, the ratio between the the principal axis and the orthogonal one standard deviations, and θ , the angle between the major axis and the

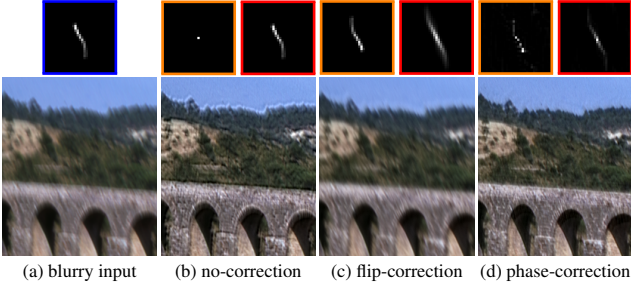


Figure 4: Kernels with negative or complex Fourier coefficients (as the one shown in blue) need to be compensated before applying our polynomial deblurring. In blue the input blur kernel k , in orange each respective correction filter c_k , while in red corrected kernels $h = c_k * k$ used in the Polynomial deblurring (b-d).

horizontal. Thus, the Gaussian blur kernel at pixel (x, y) is:

$$k(x, y) = Z \exp(-ax^2 + 2bxy + cy^2), \quad (9)$$

where $a = \frac{\cos(\theta)^2}{2\sigma_0^2} + \frac{\sin(\theta)^2}{2\rho^2\sigma_0^2}$, $b = \frac{\sin(2\theta)}{4\sigma_0^2}(\frac{1}{\rho^2} - 1)$, $c = \frac{\sin(\theta)^2}{2\sigma_0^2} + \frac{\cos(\theta)^2}{2\rho^2\sigma_0^2}$ and Z is a normalization constant so the area of the kernel is one. Although this is a rough model for arbitrary blur in images, if the blur is small, either directional or isotropic, the anisotropic Gaussian parameterization is reasonable. Figure 5(left) shows examples of Gaussian blur kernels.

4.1. From natural image model to blur estimation

Estimating a blur kernel given only an image is a challenging ill-posed problem. It is necessary to make some assumptions, for instance by using an image prior (learned from data or from a statistical or any kind of mathematical model). In this work, we focus on efficiency and require that the estimation of the blur is very fast. Thus, variational models, for instance those typically involved in blind-deconvolution approaches are prohibitively expensive. Instead, we will rely on the following rough observations about the image gradient distribution.

Assumption 1. *In a sharp image, the maximum value of the image gradient in any direction is mostly constant and roughly independent of the image.*

Assumption 2. *If a sharp image is affected by Gaussian blur, the blur level in the direction of the principal axis will be linearly related to the inverse of the maximum image gradient in the principal directions.*

Based on these assumptions we proceed as follows. We first estimate the maximum magnitude of the image derivative at all possible orientations and then take the minimum

value among them. This leads to

$$f_\theta = \min_{\psi \in [0, \pi)} f_\psi = \min_{\psi \in [0, \pi)} \max_{\mathbf{x}} |\nabla_\psi v(\mathbf{x})|, \quad (10)$$

where $v(\mathbf{x})$ is the input image, and $\nabla_\psi f(\mathbf{x}) = \nabla v(\mathbf{x}) \cdot (\cos \psi, \sin \psi)$, is the directional derivative of v at direction ψ . Then, the blur kernel parameters are

$$\theta = \arg \min_{\psi \in [0, \pi)} f_\psi, \quad \sigma_0 = \frac{c}{f_\theta} \quad \text{and} \quad \sigma_1 = \frac{c}{f_{\theta_\perp}}, \quad (11)$$

where c is a coefficient controlling the assumed linear relation between the gradient feature and the level of blur.

Observation. The estimation of the image gradient at any given image pixel introduces additional blur (since some sort of interpolation is needed). This will be in addition to the image blur that the image already has. Let us assume the blur estimation introduces an isotropic Gaussian blur of strength σ_b , then the total blur of the image will be approximately $\sigma_{0_T}^2 = \sigma_b^2 + \sigma_0^2$ (due to the semigroup property of Gaussian function). This leads to

$$\sigma_0 = \sqrt{\frac{c^2}{f_\theta^2} - \sigma_b^2}, \quad \sigma_1 = \sqrt{\frac{c^2}{f_{\theta_\perp}^2} - \sigma_b^2}, \quad (12)$$

where c and σ_b are two parameters to be calibrated.

4.2. Calibration and model validation

To calibrate the parameters c and σ_b we proceed as follows. Given a set of sharp high quality images, we simulate $K = 1000$ random Gaussian blurry images, by randomly sampling the blur space and the image set. The Gaussian blur kernels are generated by sampling random values for $\sigma_0 \in [0.3, 4]$ and $\rho \in [0.15, 1]$. Additive Gaussian white noise of standard deviation 1% is added to each simulated blurry image.

For each of the blurry images we compute the gradient features and the maximum and minimum values according to (10). The parameters c and σ_b are estimated by minimizing the mean absolute error. Figure 5 presents the calibration results. Additional details are included in the supplemental material.

5. Polyblur implementation details

In this section we describe a Polyblur implementation to allow us to achieve the performance to deblur a 12MP image on a modern mobile platform in a fraction of a second. The core parts of the algorithm are implemented using the language *Halide* [40].

Blur estimation. We follow Sec. 4.1 to estimate the blur. As the first step we normalize the image using quantiles ($q = 0.0001$ and $1 - q$) to be robust to outliers. From the image gradient we compute the directional derivative at

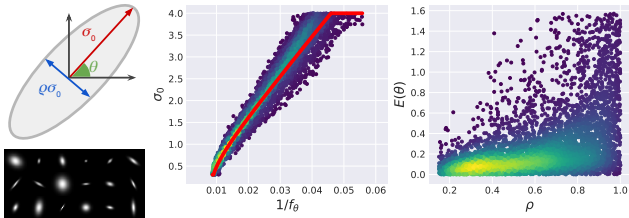


Figure 5: Gaussian blur model and examples (left). The middle plot shows the relationship between the computed gradient feature f_θ and σ_0 on simulated images, and the calibrated model (Eq. (12), red curve). The right plot shows the error on the estimation of the blur angle θ , as a function of ρ . Angle estimation error is very low for anisotropic (directional) kernels (low ρ value).

$m = 6$ angles uniformly covering $[0, \pi)$. The maximum direction of the magnitude at each angle is found and among the m maximum values, we find the minimum value and angle (f_θ, θ_0) through bicubic interpolation. Using (12) we compute σ_0 and σ_1 . A pseudo-code for the blur estimation step is included in the supplemental material.

Deblurring step. The deblurring filter has a closed form given by the estimated blur and the polynomial in (8). In the case of using a third order polynomial, the restoration filter support is roughly three times the one of the estimated base blur. Large blur kernel convolutions can be efficiently computed in Fourier domain. If the Gaussian blur is separable, the convolution can be efficiently computed in-place. In this case, we do not compute the polynomial filter and directly apply and accumulate repeated applications of the Gaussian blur as follows:

$$v_0 = a_d v, \quad v_i = k * v_{i-1} + a_{d-i} v, \quad \text{for } i=1, \dots, d, \quad (13)$$

where v is the input blurry image, k the estimated blur kernel, and a_0, \dots, a_d the deblurring polynomial coefficients, and v_d the deblurred output image. Non-separable Gaussian filtering can also be efficiently computed by two 1D Gaussian filters in non-orthogonal axis. This can further optimize our procedure.

Halo detection and removal. Halos can be generated due to misestimation of blur or more generally due to model mismatch. Halos appear at pixels where the blurry image and restored image have opposite gradients (gradient reversal). Let $v(\mathbf{x})$ be the blurry image and $\bar{v}(\mathbf{x})$ the deblurred one. Pixels with gradient reversal are those where $M(\mathbf{x}) = -\nabla v(\mathbf{x}) \cdot \nabla \bar{v}(\mathbf{x})$, is positive.

Let us compute a new image $\bar{v}_z(\mathbf{x})$ formed as a per pixel convex combination (blending) of the input image $v(\mathbf{x})$ and the deblurred one $\bar{v}(\mathbf{x})$ using a weights $z(\mathbf{x}) \in [0, 1]$,

$$v_z(\mathbf{x}) = z(\mathbf{x})v(\mathbf{x}) + (1 - z(\mathbf{x}))\bar{v}(\mathbf{x}). \quad (14)$$

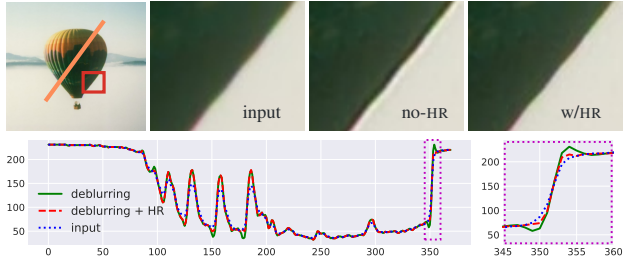


Figure 6: Halo Removal (HR). Top row shows a crop for the input image, the deblurred one, and the final merge with the halo removal step. In the bottom we show a profile (and a zoom-in on the right) of the insensitive values orthogonal to the balloon boundary (orange segment). The gradient reversal has been eliminated.

We want to avoid halos in the final image $v_z(\mathbf{x})$, but keep as much as possible of the deblurred one $\bar{v}(\mathbf{x})$. If $z(\mathbf{x})$ does not change too fast, then

$$\nabla v_z(\mathbf{x}) = z(\mathbf{x})\nabla v(\mathbf{x}) + (1 - z(\mathbf{x}))\nabla \bar{v}(\mathbf{x}). \quad (15)$$

To avoid halos on the final image we require $\nabla v(\mathbf{x}) \cdot \nabla v_z(\mathbf{x}) > 0$. Then, we get that for pixels where $M(\mathbf{x}) > 0$, having

$$z(\mathbf{x}) \leq \frac{M(\mathbf{x})}{\|\nabla v(\mathbf{x})\|^2 + M(\mathbf{x})},$$

leads to a new image that does not have any gradient reversal introduced in the deblurring step. To keep as much as possible of the deblurred image, $z(\mathbf{x})$ should be as small as possible. Then the final image is generated by adopting

$$z(\mathbf{x}) = \max\left(\frac{M(\mathbf{x})}{\|\nabla v(\mathbf{x})\|^2 + M(\mathbf{x})}, 0\right), \quad (16)$$

in the convex combination given by (14). Figure 6 shows an example of a filtered image and the halo correction.

Polyblur iterated. To remove some remaining image blur, we can re-apply Polyblur. This implies re-estimating the image blur on the previous deblurred image, and applying a new polynomial deblurring. In the next section we present some results when iterating polyblur multiple times.

6. Experiments

We carried out a series of experiments to evaluate Polyblur and compare against other blind deblurring [12, 15, 26, 36, 45, 53] and sharpening methods [14, 56]. The comparison is threefold: we compare traditional metrics such as PSNR, SSIM and perceptual ones such as LPIPS [55]; we do a visual inspection of artifacts (qualitative); and we report processing times. We also present results on images *in the wild* having mild blur. Finally, we show how Polyblur can be used to remove blur before applying an off-the-shelf

Algorithm phase	12MP	3MP	1MP
1. Blur estimation	302 (357)	88 (95)	23 (25)
2a. Polyblur (separable)	66 (194)	16 (82)	9 (35)
2b. Polyblur (Fourier)	266 (472)	35 (212)	16(134)
3. Halo removal	14 (70)	61 (20)	3 (7)

Table 1: Times in ms run on desktop(mobile). Desktop: Intel Xeon Haswell 2.3GHz, mobile: Snapdragon 855.

image superresolution deep method. Table 1 shows average execution times for each step in the Polyblur algorithm. Our method can process a 12MP image on a modern mobile platform in 600ms.

Comparison on simulated blur. We generated a mild-blur dataset by artificially blurring sharp images from the DIV2K validation dataset. Mild blur is simulated by applying a random Gaussian kernel of different sizes, shapes, and orientations ($\sigma_0 \sim \mathcal{U}[0.3, 4]$). Additive white Gaussian noise of standard deviation 1% is added on top. More details are included in the supplementary material. Polyblur produces the best results in terms of PSNR and MS-SSIM while being significantly faster than most of the other deblurring methods (Table 2). As shown in Figure 7, Polyblur leads to naturally pleasant images, while most of the compared methods introduce artifacts. The visual quality of the output results is similar to highly complex methods such as DeblurGAN-v2 [26]. Our CPU implementation of Polyblur is still 50% faster than the highly optimized mobile version of DeblurGANv2 that runs on GPU.

Method	PSNR	MS-SSIM	LPIPS	Time
SRN [45]	27.58	0.948	0.304	75-152 [†]
SparseDeb [53]	27.48	0.940	0.296	> 5000
DeblurGANv2 [26]	29.79	0.963	0.213	350 [†]
DeblurGANv2m [26]	29.53	0.958	0.209	60 [†]
Spectral [12]	27.14	0.950	0.230	> 5000
Deblur-10 [36]	27.31	0.945	0.263	> 5000
GLAS [56]	28.15	0.957	0.284	> 5000
GuidFilt [14]	26.98	0.934	0.282	80
ConvDeb [15]*	27.08	0.938	0.238	90
Polyblur-1it	30.38	0.968	0.236	42
Polyblur-2it	30.06	0.964	0.255	84
Polyblur-3it	29.44	0.955	0.269	126
Blurry-noisy	29.31	0.956	0.245	-

Table 2: Mild deblurring on the synthetic dataset generated from DIV2K. Lower LPIPS values imply better quality. Polyblur- N it indicates applying Polyblur N times. ConvDeb [15]* did not produce reasonable results in 32/100 images (average values are computed in the rest). Times are in ms (for a 1MP image), and we present them here as an indicative reference. [†] indicates GPU.



Figure 7: Comparison of Polyblur with other deblurring and adaptive sharpening methods on synthetically blurred DIV2K dataset.

Dealing with noise and compression artifacts. If computational resources are available, a prefiltering step separating noise-like structure from the rest can be applied. If the input image is very noisy or has compression artifacts, this prefiltering step will keep Polyblur from amplifying artifacts present in the image. Since the residual image can be added back at the end, this step does not need to be carried out by a state-of-the-art denoiser. Fig. 8 shows an example of Polyblur on a noisy and compressed image. We evaluated two alternatives, the Pull-Push denoiser [17] and the Domain Transform [11] edge-preserving filter. In both cases we achieve the desired deblurring, and a pleasant result.

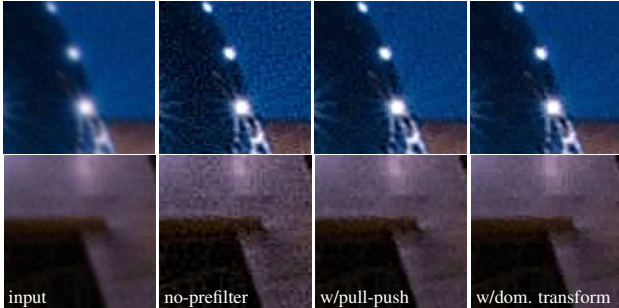


Figure 8: Pre-filtering. When the input image presents noise and other artifacts, Polyblur can amplify artifacts. As a pre-step, we may apply any filter that separates high-frequency texture and other details [11, 17], apply Polyblur ($\alpha = 6$, $b = 1$), and finally add back the residual.

Results on images *in the wild*. In Figure 1 we present a selection of results of Polyblur applied to some images in the wild. As shown, Polyblur manages to remove mild blur, as the one present in most images, without introducing any new artifacts. Please refer to the supplemental material for comparison with other state-of-the-art deblurring and sharpening methods.

Deblurring before super-resolution. Single image super-resolution has seen remarkable progress in the last few years mostly due the use of deep models trained on image datasets. The common practice [52] is to simulate low-resolution training images by simply applying a bicubic downsampling operator. Unfortunately, inference performance suffers significantly if images do not tightly follow the training distribution. We evaluate the performance of applying Polyblur as a pre-step before using an off-the-shelf deep network for doing $4\times$ image upscaling. We trained from scratch an EDSR [30] network with 32 layers and 64 filters using DIV2K training dataset. We compare against KernelGAN [2] and the Correction filter introduced in [16]. Figure 9 shows examples of applying Polyblur before upscaling the image. Table 3 shows a quantitative comparison of our approach and the competitors. Polyblur produces the best quantitative and qualitative results.

7. Conclusion

We introduced a highly efficient algorithm for estimating and removing mild blur that is ubiquitously present in many captured images (especially on handheld devices). A parametric blur kernel is first estimated using simple gradient features that encode the direction and intensity of the blur. The estimated blur is then removed by combining multiple applications of the blur kernel in a well founded way that allows us to approximate the inverse while controlling the noise amplification. Our experiments show that, in the context of mild blur, the algorithm produces similar

Method	PSNR	SSIM
Bicubic	25.354	0.6775
EDSR [30]	25.628	0.6971
KernelGAN [2]	26.810	0.7316
CorrectionFilter[16] + EDSR	26.204	0.736
Polyblur-1it + EDSR	26.966	0.7396
Polyblur-2it + EDSR	27.115	0.7452
Polyblur-3it + EDSR	26.955	0.7368

Table 3: $4\times$ Super-resolution on DIV2K dataset [2]. Polyblur- N it indicates applying Polyblur N times. PSNR and SSIM values are directly taken from [2, 16]. In red font the best method, in blue the second best.

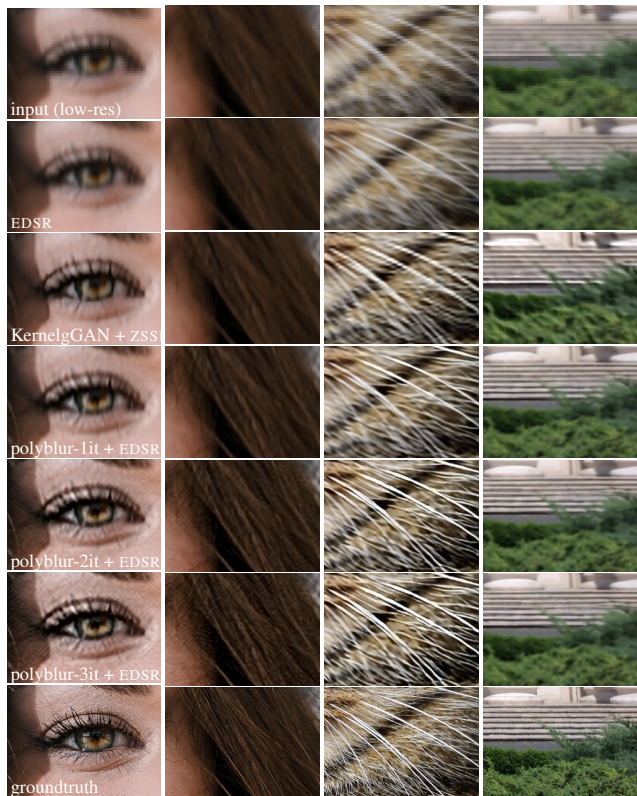


Figure 9: Image $4\times$ super-resolution using an off-of-the-shelf deep SISR model with *unknown* PSF (EDSR [30]). More results are given in the supplementary material.

or better results than other state-of-the-art image deblurring methods while being significantly faster. The whole deblurring process runs in a fraction of a second on a 12MP image on a modern mobile platform. Our method can be used to blindly correct blur before applying an off-the-shelf deep super-resolution model leading to superior results than other computationally demanding techniques. As future work, we would like to explore how to extend our method to address stronger blurs while maintaining the high efficiency of the algorithm.

References

- [1] Jérémy Anger, Gabriele Facciolo, and Mauricio Delbracio. Modeling realistic degradations in non-blind deconvolution. In *2018 25th IEEE International Conference on Image Processing (ICIP)*, pages 978–982. IEEE, 2018. 2
- [2] Sefi Bell-Kligler, Assaf Shocher, and Michal Irani. Blind super-resolution kernel estimation using an internal-gan. In *Advances in Neural Information Processing Systems*, pages 284–293, 2019. 8
- [3] Antoni Buades, Bartomeu Coll, and J-M Morel. A non-local algorithm for image denoising. In *2005 IEEE Computer Society Conference on Computer Vision and Pattern Recognition (CVPR'05)*, volume 2, pages 60–65. IEEE, 2005. 2
- [4] Jian-Feng Cai, Hui Ji, Chaoqiang Liu, and Zuowei Shen. Blind motion deblurring from a single image using sparse approximation. In *2009 IEEE Conference on Computer Vision and Pattern Recognition*, pages 104–111. IEEE, 2009. 2
- [5] Ayan Chakrabarti. A neural approach to blind motion deblurring. In *European conference on computer vision*, pages 221–235. Springer, 2016. 3
- [6] Tony F Chan and Chiu-Kwong Wong. Total variation blind deconvolution. *IEEE transactions on Image Processing*, 7(3):370–375, 1998. 2
- [7] Liang Chen, Faming Fang, Tingting Wang, and Guixu Zhang. Blind image deblurring with local maximum gradient prior. In *Proceedings of the IEEE Conference on Computer Vision and Pattern Recognition*, pages 1742–1750, 2019. 2
- [8] Sunghyun Cho and Seungyong Lee. Fast motion deblurring. In *ACM SIGGRAPH Asia 2009 papers*, pages 1–8. 2009. 2
- [9] Rob Fergus, Barun Singh, Aaron Hertzmann, Sam T Roweis, and William T Freeman. Removing camera shake from a single photograph. In *ACM SIGGRAPH 2006 Papers*, pages 787–794. 2006. 1, 2
- [10] Hongyun Gao, Xin Tao, Xiaoyong Shen, and Jiaya Jia. Dynamic scene deblurring with parameter selective sharing and nested skip connections. In *Proceedings of the IEEE Conference on Computer Vision and Pattern Recognition*, pages 3848–3856, 2019. 1, 3
- [11] Eduardo SL Gastal and Manuel M Oliveira. Domain transform for edge-aware image and video processing. In *ACM SIGGRAPH 2011 papers*, pages 1–12. 2011. 7, 8
- [12] Amit Goldstein and Raanan Fattal. Blur-kernel estimation from spectral irregularities. In *European Conference on Computer Vision*, pages 622–635. Springer, 2012. 6, 7
- [13] Kaiming He, Jian Sun, and Xiaoou Tang. Guided image filtering. In *European conference on computer vision*, pages 1–14. Springer, 2010. 1, 2
- [14] Kaiming He, Jian Sun, and Xiaoou Tang. Guided image filtering. *IEEE transactions on pattern analysis and machine intelligence*, 35(6):1397–1409, 2012. 6, 7
- [15] Mahdi S Hosseini and Konstantinos N Plataniotis. Convolutional deblurring for natural imaging. *IEEE Transactions on Image Processing*, 29:250–264, 2019. 6, 7
- [16] Shady Abu Hussein, Tom Tirer, and Raja Giryes. Correction filter for single image super-resolution: Robustifying off-the-shelf deep super-resolvers. In *Proceedings of the IEEE/CVF Conference on Computer Vision and Pattern Recognition*, pages 1428–1437, 2020. 8
- [17] John R Isidoro and Peyman Milanfar. Pull-push non-local means with guided and burst filtering capabilities. In *Denoising of Photographic Images and Video*, pages 267–294. Springer, 2018. 7, 8
- [18] Meiguang Jin, Stefan Roth, and Paolo Favaro. Normalized blind deconvolution. In *Proceedings of the European Conference on Computer Vision (ECCV)*, pages 668–684, 2018. 2
- [19] J Kaiser and R Hamming. Sharpening the response of a symmetric nonrecursive filter by multiple use of the same filter. *IEEE Transactions on Acoustics, Speech, and Signal Processing*, 25(5):415–422, 1977. 3
- [20] Sang Ho Kim and Jan P Allebach. Optimal unsharp mask for image sharpening and noise removal. *Journal of Electronic Imaging*, 14(2):023005, 2005. 2
- [21] Leslie SG Kováczny and Horace M Joseph. Image processing. *Proceedings of the IRE*, 43(5):560–570, 1955. 1
- [22] Dilip Krishnan and Rob Fergus. Fast image deconvolution using hyper-laplacian priors. In *Advances in neural information processing systems*, pages 1033–1041, 2009. 2
- [23] Dilip Krishnan, Terence Tay, and Rob Fergus. Blind deconvolution using a normalized sparsity measure. In *CVPR 2011*, pages 233–240. IEEE, 2011. 2
- [24] Deepa Kundur and Dimitrios Hatzinakos. Blind image deconvolution. *IEEE signal processing magazine*, 13(3):43–64, 1996. 1, 2
- [25] Orest Kupyn, Volodymyr Budzan, Mykola Mykhailych, Dmytro Mishkin, and Jiří Matas. Deblurgan: Blind motion deblurring using conditional adversarial networks. In *Proceedings of the IEEE conference on computer vision and pattern recognition*, pages 8183–8192, 2018. 1, 3
- [26] Orest Kupyn, Tetiana Martyniuk, Junru Wu, and Zhangyang Wang. Deblurgan-v2: Deblurring (orders-of-magnitude) faster and better. In *Proceedings of the IEEE International Conference on Computer Vision*, pages 8878–8887, 2019. 1, 3, 6, 7
- [27] Wei-Sheng Lai, Jia-Bin Huang, Zhe Hu, Narendra Ahuja, and Ming-Hsuan Yang. A comparative study for single image blind deblurring. In *Proceedings of the IEEE Conference on Computer Vision and Pattern Recognition*, pages 1701–1709, 2016. 1, 2
- [28] Anat Levin, Yair Weiss, Fredo Durand, and William T Freeman. Understanding and evaluating blind deconvolution algorithms. In *2009 IEEE Conference on Computer Vision and Pattern Recognition*, pages 1964–1971. IEEE, 2009. 1, 2
- [29] Anat Levin, Yair Weiss, Fredo Durand, and William T Freeman. Efficient marginal likelihood optimization in blind deconvolution. In *CVPR 2011*, pages 2657–2664. IEEE, 2011. 2
- [30] Bee Lim, Sanghyun Son, Heewon Kim, Seungjun Nah, and Kyoung Mu Lee. Enhanced deep residual networks for single image super-resolution. In *Proceedings of the IEEE conference on computer vision and pattern recognition workshops*, pages 136–144, 2017. 8

- [31] Tomer Michaeli and Michal Irani. Blind deblurring using internal patch recurrence. In *European conference on computer vision*, pages 783–798. Springer, 2014. 2
- [32] Peyman Milanfar. A tour of modern image filtering: New insights and methods, both practical and theoretical. *IEEE signal processing magazine*, 30(1):106–128, 2012. 2
- [33] Peyman Milanfar. Rendition: Reclaiming what a black box takes away. *SIAM Journal on Imaging Sciences*, 11(4):2722–2756, 2018. 3
- [34] Seungjun Nah, Sanghyun Son, Radu Timofte, and Kyoung Mu Lee. Ntire 2020 challenge on image and video deblurring. In *Proceedings of the IEEE/CVF Conference on Computer Vision and Pattern Recognition Workshops*, pages 416–417, 2020. 3
- [35] Jinshan Pan, Zhe Hu, Zhixun Su, and Ming-Hsuan Yang. Deblurring text images via l0-regularized intensity and gradient prior. In *Proceedings of the IEEE Conference on Computer Vision and Pattern Recognition*, pages 2901–2908, 2014. 2
- [36] Jinshan Pan, Zhe Hu, Zhixun Su, and Ming-Hsuan Yang. l₀-regularized intensity and gradient prior for deblurring text images and beyond. *IEEE transactions on pattern analysis and machine intelligence*, 39(2):342–355, 2016. 6, 7
- [37] Jinshan Pan, Deqing Sun, Hanspeter Pfister, and Ming-Hsuan Yang. Deblurring images via dark channel prior. *IEEE transactions on pattern analysis and machine intelligence*, 40(10):2315–2328, 2017. 2
- [38] Daniele Perrone and Paolo Favaro. Total variation blind deconvolution: The devil is in the details. In *Proceedings of the IEEE Conference on Computer Vision and Pattern Recognition*, pages 2909–2916, 2014. 1, 2
- [39] Andrea Polesel, Giovanni Ramponi, and V John Mathews. Image enhancement via adaptive unsharp masking. *IEEE transactions on image processing*, 9(3):505–510, 2000. 2
- [40] Jonathan Ragan-Kelley, Andrew Adams, Sylvain Paris, Marc Levoy, Saman Amarasinghe, and Frédo Durand. Decoupling algorithms from schedules for easy optimization of image processing pipelines. *ACM Transactions on Graphics (TOG)*, 31(4):1–12, 2012. 5
- [41] Qi Shan, Jiaya Jia, and Aseem Agarwala. High-quality motion deblurring from a single image. *Acm transactions on graphics (tog)*, 27(3):1–10, 2008. 1, 2
- [42] Shuo Chen Su, Mauricio Delbracio, Jue Wang, Guillermo Sapiro, Wolfgang Heidrich, and Oliver Wang. Deep video deblurring for hand-held cameras. In *Proceedings of the IEEE Conference on Computer Vision and Pattern Recognition*, pages 1279–1288, 2017. 1, 3
- [43] Jian Sun, Wenfei Cao, Zongben Xu, and Jean Ponce. Learning a convolutional neural network for non-uniform motion blur removal. In *Proceedings of the IEEE Conference on Computer Vision and Pattern Recognition*, pages 769–777, 2015. 3
- [44] Hossein Talebi and Peyman Milanfar. Fast multilayer laplacian enhancement. *IEEE Transactions on Computational Imaging*, 2(4):496–509, 2016. 1, 2
- [45] Xin Tao, Hongyun Gao, Xiaoyong Shen, Jue Wang, and Jiaya Jia. Scale-recurrent network for deep image deblurring. In *Proceedings of the IEEE Conference on Computer Vision and Pattern Recognition*, pages 8174–8182, 2018. 1, 3, 6, 7
- [46] Xin Tao, Chao Zhou, Xiaoyong Shen, Jue Wang, and Jiaya Jia. Zero-order reverse filtering. In *Proceedings of the IEEE International Conference on Computer Vision*, pages 222–230, 2017. 3
- [47] Carlo Tomasi and Roberto Manduchi. Bilateral filtering for gray and color images. In *Sixth international conference on computer vision (IEEE Cat. No. 98CH36271)*, pages 839–846. IEEE, 1998. 2
- [48] Patrick Wieschollek, Michael Hirsch, Bernhard Scholkopf, and Hendrik Lensch. Learning blind motion deblurring. In *Proceedings of the IEEE International Conference on Computer Vision*, pages 231–240, 2017. 1, 3
- [49] Patrick Wieschollek, Bernhard Schölkopf, Hendrik PA Lensch, and Michael Hirsch. End-to-end learning for image burst deblurring. In *asian conference on computer vision*, pages 35–51. Springer, 2016. 3
- [50] Li Xu and Jiaya Jia. Two-phase kernel estimation for robust motion deblurring. In *European conference on computer vision*, pages 157–170. Springer, 2010. 2
- [51] Li Xu, Shicheng Zheng, and Jiaya Jia. Unnatural l0 sparse representation for natural image deblurring. In *Proceedings of the IEEE conference on computer vision and pattern recognition*, pages 1107–1114, 2013. 2
- [52] Wenming Yang, Xuechen Zhang, Yapeng Tian, Wei Wang, Jing-Hao Xue, and Qingmin Liao. Deep learning for single image super-resolution: A brief review. *IEEE Transactions on Multimedia*, 21(12):3106–3121, 2019. 8
- [53] Haichao Zhang, David Wipf, and Yanning Zhang. Multi-image blind deblurring using a coupled adaptive sparse prior. In *Proceedings of the IEEE Conference on Computer Vision and Pattern Recognition*, pages 1051–1058, 2013. 6, 7
- [54] Kaihao Zhang, Wenhan Luo, Yiran Zhong, Lin Ma, Bjorn Stenger, Wei Liu, and Hongdong Li. Deblurring by realistic blurring. In *Proceedings of the IEEE/CVF Conference on Computer Vision and Pattern Recognition*, pages 2737–2746, 2020. 1, 3
- [55] Richard Zhang, Phillip Isola, Alexei A Efros, Eli Shechtman, and Oliver Wang. The unreasonable effectiveness of deep features as a perceptual metric. In *Proceedings of the IEEE conference on computer vision and pattern recognition*, pages 586–595, 2018. 6
- [56] Xiang Zhu and Peyman Milanfar. Restoration for weakly blurred and strongly noisy images. In *2011 IEEE Workshop on Applications of Computer Vision (WACV)*, pages 103–109. IEEE, 2011. 2, 6, 7